Channel response to an extreme flood and sediment pulse in a mixed bedrock and gravel-bed river

Abstract (300 word limit)

We exploit a natural experiment caused by a high-magnitude flood (~500 yr recurrence interval) and sediment slug derived from more than 2,500 concurrent landslides to explore the influence of valley-scale geomorphic controls on sediment slug evolution and the impact of sediment slug passage and emplacement on channel stability and channel form. Movement of sediment slugs is a crucial process that shapes gravel bed rivers and alluvial valleys and is an important mechanism of downstream bed material transport, while changes in bed material transport rate that occur during slug emplacement can trigger channel responses including increases in river channel lateral mobility, channel widening, and increase in alluvial bar dominance.

Multitemporal LiDAR and aerial photos bracketing the flood event, which occurred in 2007 on the Chehalis River in SW Washington State, USA, document the channel response to this event with high spatial and temporal definition. The sediment slug behaved as a Gilbert Wave, with both channel aggradation and sequestration of large

volumes of material in floodplains of headwaters reaches and reaches where confined valleys enter into broad alluvial valleys. Peculiarities of the valley form through which slugs in two separate sub basins moved highlight the important role channel and channel-floodplain connectivity play in governing downstream movement of sediment slug material.

Finally, channel response to the high-magnitude flood and increase in bed material sediment transport rate illustrate the connection between bed material transport and channel form. The channel widened, lateral channel mobility increased, and relative importance of bars within the active channel increased in all reaches in the study area. But the response scaled tightly with the relative amount of bed material sediment transport through individual reaches, indicating that the geomorphic effectiveness of the flood was conditioned by the simultaneous introduction of a sediment slug to the channel network.

Introduction

In gravel bed rivers, bed material transport is the primary process that shapes channel form (Church, 2006) and controls river channel lateral mobility (Wickert et al., 2013; Constantine et al., 2014). The introduction and dispersal of bed material slugs are a particularly important instance of bed material transport, which can cause dynamic changes in river channel morphodynamics (e.g. Nicholas et al., 1995; James, 2010).

Past work to document the behavior of large sediment slugs has focused on retrospective studies of bed waves using terrain markers, stream surveys (including specific gauge analysis), and sediment budget analysis (e.g. James, 1989, 1991, 1993;

Marron, 1992; Meade, 1982); while work resolving sediment slug evolution in multiple time steps has focused on small-scale sediment slugs such as individual landslides (Sutherland et al., 2002; Cui et al., 2003; Hoffman and Gabet, 2007).

Retrospective studies of mega-scale and larger sediment slugs (sensu. Nicholas et al., 1995) have highlighted the importance of overbank sediment storage in creating asymmetrical bed-wave and sediment-wave dynamics (Major et al., 1996, 2000; Major, 2004; Gran and Montgomery, 2005) and long relaxation times before disturbed systems return to pre-disturbance or new equilibrium conditions. This situation, where overbank storage provides a key role in mediating sediment flux, resulting in asymmetry between the early passage of a bed wave (as measured in changes in the local bed elevation through time) and a temporally skewed sediment wave (as measured in elevated sediment flux), has been given the name ‘Gilbert Wave’ by James (2006, 2010), in reference to the classic case history of the impact of hydraulic mining debris in the Sacramento Basin.

The behavior of a megaslugs in natural rivers is strongly governed by the virtual velocity of the slug material and connectivity, both lateral between channel and floodplain (e.g. Croke et al., 2013) and longitudinal between channel segments (e.g. Benda and Dunne, 1997; Hooke, 2003; Nelson and Church, 2012; Kuo and Brierley, 2014). It is important to recognize, however, that downstream sediment connectivity is grainsize specific and that sediment slug derived material may be separated by transport processes and emplaced simultaneously in multiple river segments.

A large scale natural experiment, allowing observation of the evolution and impact of a slug of large megaslug in unprecedented detail, was set up when a large flood and over

2,500 individual mass wasting events occurred in the upper Chehalis Basin of southwestern Washington State, USA in early December, 2007. Abundant remote sensing data, including multi-temporal LiDAR data and frequent aerial photo coverage, document the channel response to this event with high spatial and temporal definition. Here, we exploit this natural experiment to explore the influence of valley-scale geomorphic controls on sediment slug evolution and the impact of sediment slug passage and emplacement on channel stability and morphology.

The Upper Chehalis Basin and December 2007 Storm Event

Basin Context

The upper Chehalis Basin (Figure 1), includes the upper mainstem Chehalis, South Fork Chehalis, and Stillman Creek sub basins. This portion of the Chehalis drains approximately 980 km^2 of the Northern and Eastern slopes of the Willapa Hills, which have a maximum elevation in the basin of 954 m. They are intensively managed for timber production and dominantly underlain by a combination of Eocene basalt, which contribute cobble, gravel, and fines to streams and Eocene-Pliocene clastic marine sedimentary rocks, which are generally friable and dominantly contribute sand to streams (Logan, 1987; Walsh, 1987). All three subject streams abruptly debouche from confined valleys in the Willapa Hills to broad alluvial valleys with substantially lower gradient (Figure 2).

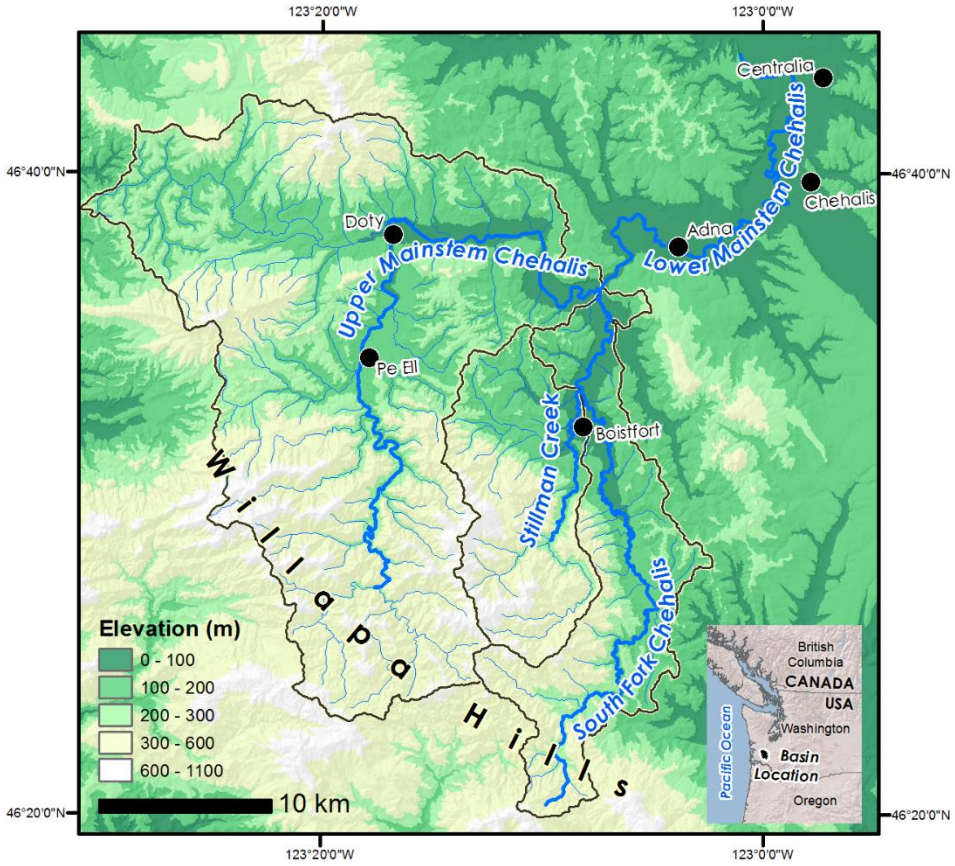

Figure 1: Upper Chehalis Basin overview. Elevation Data USGS 30 m DEM (Gesch et al., 2009).

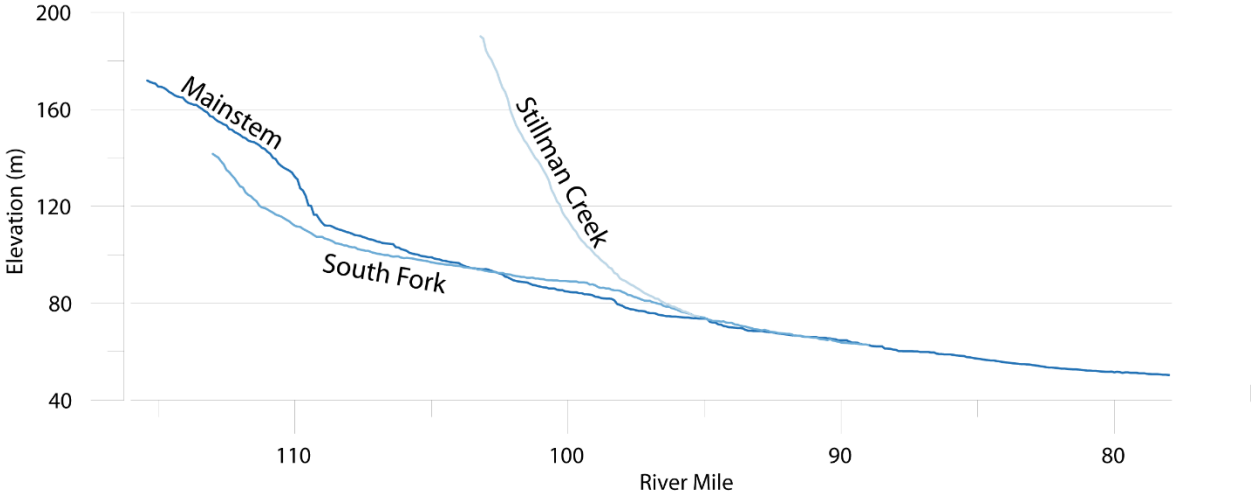

Figure 2: Slope and elevation profiles for the subject streams.

The December 2007 Storm: High Magnitude Flood and Widespread Landslides

During the period of December 1-3, 2007, heavy rains and rapid snow melt in the upper Chehalis Basin (Figure 1) caused extreme flooding on the Chehalis River and tributaries and triggered widespread mass wasting in the river's watershed. Nearly half a meter of precipitation fell at rainfall gages in the Willapa Hills (Mote et al., 2008) generating a high-magnitude flood (estimated to be on the order of a 500 year recurrence interval). The flood swamped gauging equipment, and so the peak instantaneous discharge was estimated to have been 1,790 $m^3 s^{-1}$ from high-water marks at Doty (Figure 1), which is more than twice the previous flood of record at that gauge (USGS, 2008). Two significant (>10 yr recurrence interval) floods occurred following the 2007 event in 2009 and 2012 (Figure 3).

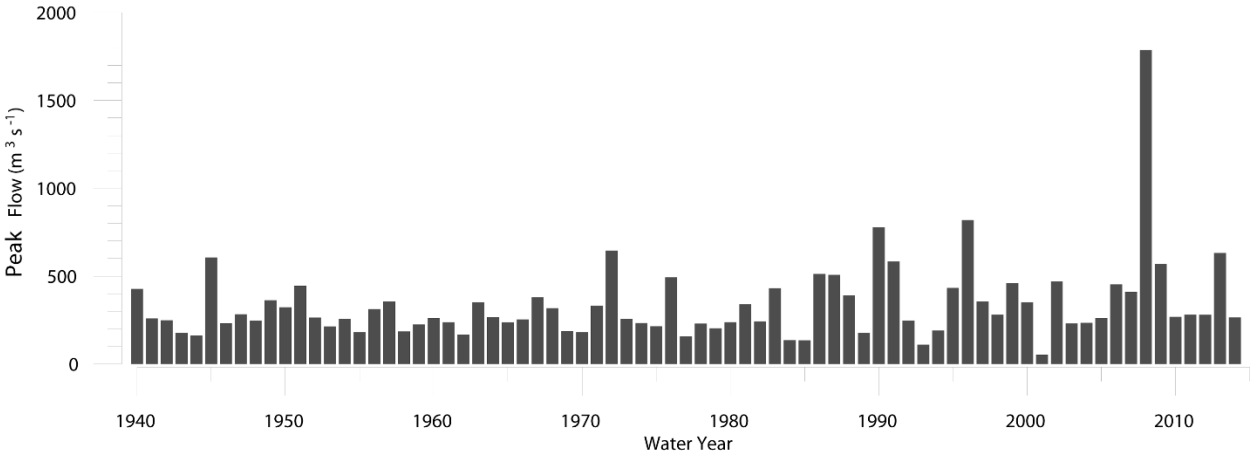

Figure 3: Chehalis River at Doty (USGS Gauge 12030000) annual instantaneous flow peaks.

Storm saturated soils gave way in over 2,500 landslides in the Upper Chehalis Basin (

Figure 4) (Sarikhan et al., 2008; DNR, 2010; Turner et al., 2010; Whittaker and McShane, 2012; Lingley et al., 2013). These slides were mostly shallow rapid slides or debris torrents, originating in areas of recent forest harvest and along forestry roads (Turner et al., 2010; Whittaker and McShane, 2012) and terminating in the channel or floodplain of the Chehalis River and tributaries.

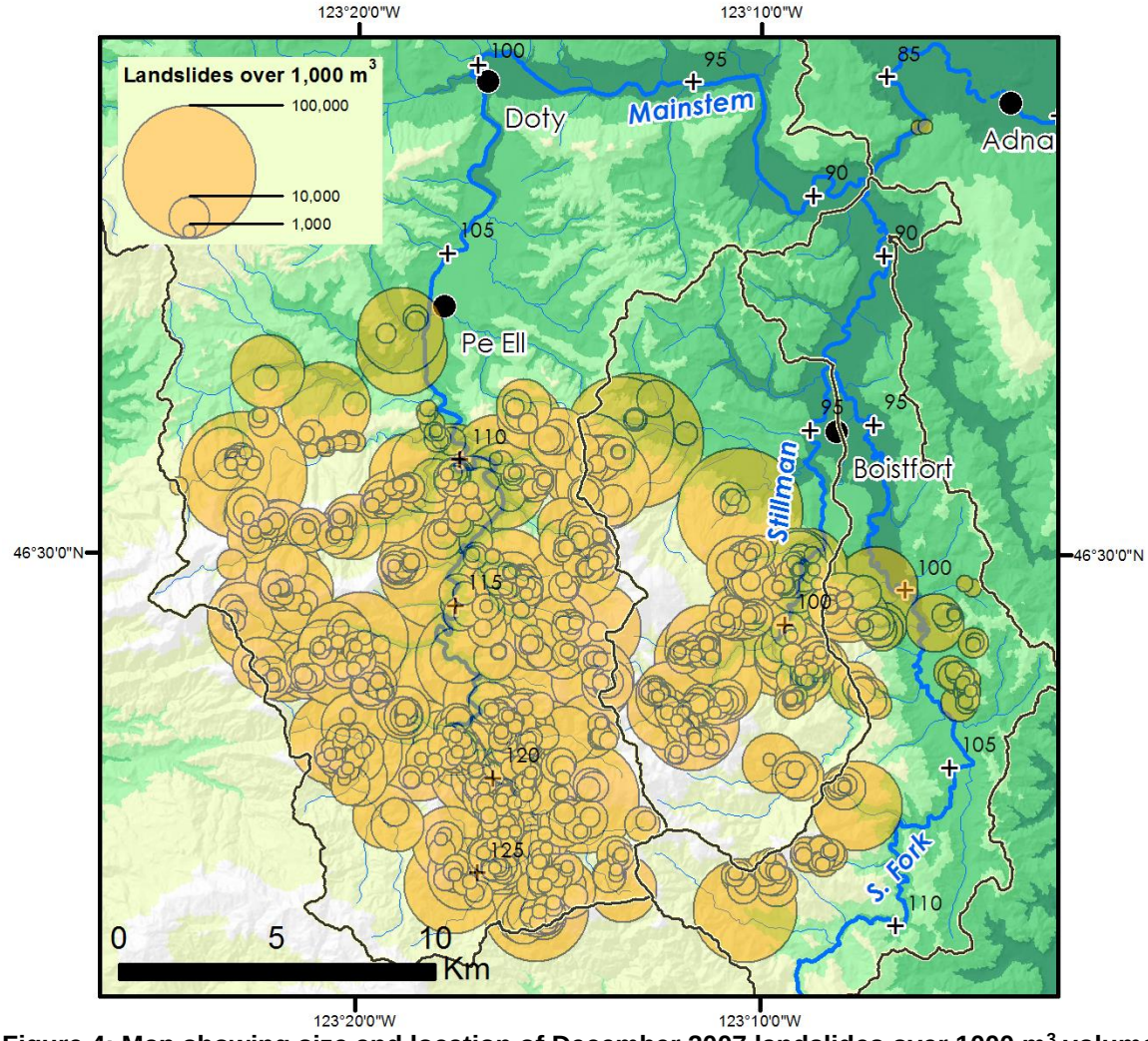

Figure 4: Map showing size and location of December 2007 landslides over 1000 m^3 volume.

Airborne LiDAR elevation data had been acquired in 2005, prior to the event, covering much of the area of the mainstem river and tributaries, and were acquired again in 2012 (PSLC, 2005, 2012); additionally, aerial orthophotos with complete coverage of the study area were acquired in 1990 (USGS), 2006, 2009, and 2011, and 2013 (USDA).

The availability of these data sources bracketing this extreme event provides the opportunity to examine channel response to an extreme flow and sedimentation event. In particular, this case study gives the opportunity to observe details of the early-stage evolution of a large megaslug.

Methods

Landslide Volume and Texture

Landslide volumes were determined by maps delineating slide area, compiled from oblique aerial photos shortly after the 2007 event and subsequent orthophotos, and ground observations to determine typical depths. The Washington Department of Natural Resources (DNR) conducted an aerial reconnaissance to map landslides in parts of the Chehalis River basin following the 2007 storms (Sarikhan et al., 2008) and distributed these data in a GIS shapefile (DNR, 2010). This shapefile was compared to 2008 orthophotos (DNR, 2008) and edited to provide an updated coverage of landslides from the 2007 storm. This coverage was annotated with estimated percent delivery to a stream for each slide, based on slide deposit proximity to mapped streams, and percent vegetative cover in 2008 and 2013 to determine revegetation and stabilization of the slide scars through time.

Field observations to evaluate typical slide depths and texture were collected in September 2011 along 20 miles of the Weyerhaeuser 1000 mainline road, which follows the mainstem Chehalis upstream of Pe Ell (

Figure 4). Slides were classified into two categories: debris slides and debris torrents. Slide depths and connectivity of the slide to the channel network were estimated for each slide that crossed the road or was readily visible. The results of this assessment were extrapolated through the study basin based on landslide area and type to estimate the volume of sediment contributed to the channel network. The procedure multiplied the area of each mapped landslide by the average depth for that type of slide and estimated delivery ratio. Slide volumes were converted to weight using an average bulk density of 1.04 t m^{-3} (USDA NRCS, 2013).

Sediment inputs from the landslides were partitioned into bedload and suspended load based on grain size properties of the average grain size distribution of three grab samples from landslides that crossed the Weyerhaeuer 1000 mainline road and the texture of dominant soils in the basin (USDA NRCS, 2013).

Channel Response

LiDAR Differencing

LiDAR data from 2005 and 2012 (PSLC, 2005, 2012) allows evaluation of both local patterns of erosion and deposition and the total change in sediment storage within the study reaches. Detection of geomorphic change between raster surfaces is a somewhat complex process that depends on the confidence in elevation estimates for each individual raster (e.g. Wheaton et al., 2010). To help address this, the analysis used a

simple and conservative method to filter out DEM uncertainty and find areas of "real change." First, all areas with absolute change in magnitude < 30 cm were filtered out based on the assumption that these changes are due to noise in the LiDAR data or due to local agricultural grading. Second, the uncertainty (u) for each DEM cell was defined as:

$$u = x \text{ Tan } \alpha \quad (1)$$

where x is the DEM cell size and α is the local slope. Cells were excluded from the analysis when the estimated change was less than the uncertainty for either compared raster. The resulting elevation change map shows areas of erosion and deposition and can be used to estimate the total change in storage component of the sediment budget.

Aerial Photo Analysis

Wetted channel and bar positions were delineated from aerial orthophotos acquired in 1990 (1m panchromatic, USGS DOQ), 2006, 2009, 2011, and 2013 (1 m color, USDA Farm Service Agency NAIP). Additionally, the position of the 2012 wetted channel was delineated from the LiDAR data. Channel conditions in 2006 and change from 1990 and 2006 —a period with typical hydrologic conditions (Figure 3) — were used as a baseline against which conditions and changes following the 2007 event could be compared.

Flows at the time of aerial photo acquisition ranged from 0.9 to 2.6 $m^3 s^{-1}$ (Table 1), which are all very low compared to the mean annual flow of 16.3 $m^3 s^{-1}$ and typical flood flows of greater than 140 $m^3 s^{-1}$. For each year prior to 2013, three classes of land cover were manually delineated: wetted channel, unvegetated bars, and areas outside of the active channel (hereafter "floodplain" although this may include some upland areas).

This mapping directly yields some basic morphologic parameters, including active channel width, proportion bar area, and low-flow wetted channel width. The 2013 dataset became available after the channel delineation was complete, but local observations from this dataset supplement the analysis.

Morphodynamic Analysis

Combining the LiDAR differencing and morphologic mapping for each period between aerial photos yields a picture of the morphodynamics in each reach. A geographic union of the land cover class polygons gives a view of surface state change through time, including areas of erosion (floodplain to wetted, floodplain to bar, and bar to wetted), accretion (wetted to bar, wetted to floodplain, and bar to floodplain), and no change. These changes are then combined with the LiDAR difference map to show the total volume of material eroded and deposited in the 2006 channel, in the area eroded between 2006 and 2011, and on the floodplain.

An additional set of useful descriptive metrics derived from the above analysis includes reach-average erosion, deposition, and vegetation colonization rates through time.

Bed Material Grainsize

The grain size distributions of 28 gravel/cobble bars along the Chehalis River and 5 bars along the South Fork Chehalis River were sampled during September 2010 to characterize the bed material through the study area at that time. Unfortunately, no grain size data are available from prior to the 2007 storm. Both armor and sub-armor layer samples were taken from bar head locations believed to be representative of mobile bed material (e.g. Klingeman and Emmett, 1982; Parker et al., 1982).

The armor layer sample followed the Wolman (1954) pebble count method. The sub-armor layer sample was taken by scraping away the armor layer and excavating approximately 50 kg of underlying material by shovel. Particles larger than 32 mm from the sub-armor layer were sorted and weighed in the field, and smaller fractions were retained for laboratory sieve analysis.

Bed Elevation

Changes in river bed elevation at selected locations were evaluated with specific gauge analysis at three sites in the upper Chehalis Basin. These were compiled for three USGS gauges in the study area, two on the mainstem at Doty and Adna (Figure 1), and one on the SF Chehalis River above the confluence with Stillman Creek (Wildwood). Stage records for the Chehalis River gauges were filtered for flows between 1.7 and 2.0 $m^3 s^{-1}$ at Doty (only stage is recorded at Adna) and for the South Fork for flows between 0.4 and 0.5 $m^3 s^{-1}$.

Study Reach Delineation

The results and discussion are organized at the scale of study reaches that were selected to characterize the channel response along the profile of the Chehalis and tributaries based on notable changes in valley morphology (Figure 5). Analysis subreaches were defined within some of these reaches at breaks in data availability or more subtle changes in morphology.

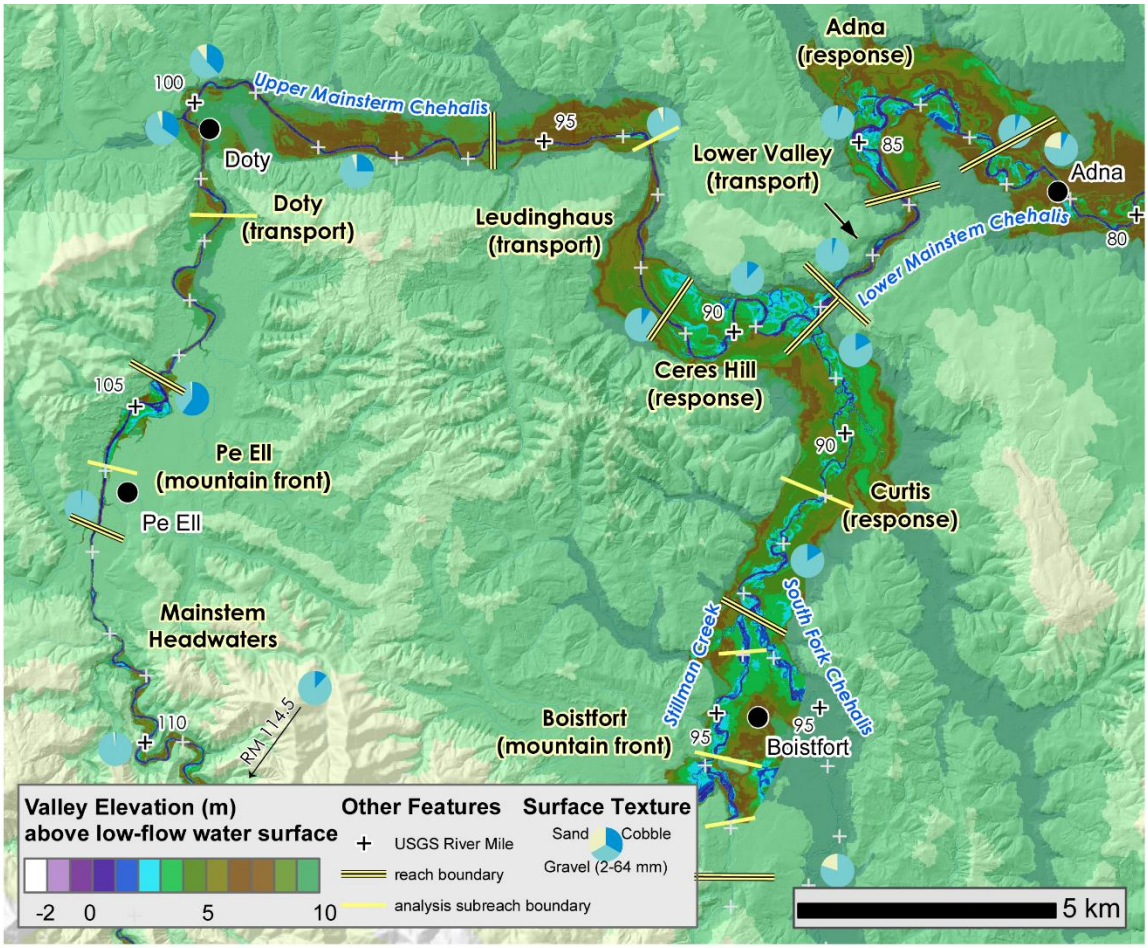

Figure 5: Reach locations and valley elevation relative to the low-flow water surface, created using the 2012 LiDAR dataset following the method of Jones (2006), except upstream of Pe-Ell where the 2008 LiDAR dataset was utilized. Note prominent constrictions at RM 101, 93.5, and 87 and relatively incised nature of the mainstem Chehalis above RM 90, with the exception of the small open area in the vicinity of RM 105.

One reach (South Fork Headwaters) was selected to illustrate the channel response in a sedimentation zone of a low-order tributary stream directly coupled to mass wasting inputs. It is located on Hanian Creek, a 3rd order stream tributary to the S.F. Chehalis River and illustrates a typical headwaters sedimentation reach response. The reach has a locally relatively low gradient (3%) and is upstream of a constriction where the valley width decreases from approximately 100 m to approximately 10m. No LiDAR data were available at this site and so interpretation is based only on aerial photos.

Two reaches, Boistfort on Stillman Creek and Pe Ell on the mainstem Chehalis, represent channel response at the mountain front where the streams exit the Willapa Hills. The bed material in both of these reaches is dominated by cobble-sized material. The Boistfort reach on Stillman Creek extends from its confluence with the S.F. Chehalis River to the mountain front. Upstream of the reach Stillman Creek flows through a narrow valley and has a gradient of approximately 2%. The Boistfort Reach flows through a 150 m wide floodplain slightly incised into a large alluvial fan, which protrudes into the larger S.F. Chehalis River Valley. The reaches' slope gradually decreases from ~1% at the head of the fan to ~0.3% at the confluence of Stillman Creek and the South Fork Chehalis. Bridges and their abutments locally confine the flow, but there are no major bedrock controls on the channel gradient or alluvial valley width. In contrast, the Pe Ell reach on the mainstem Chehalis occurs downstream of an abrupt break in slope where the river gradient abruptly decreases from approximately 0.5% to less than 0.1% (River Mile 107 in Figure 2). It includes a locally wide floodplain zone between the confined upstream valley and incised channel downstream (Figure 5).

Downstream of the mountain front reaches were classified either as transport reaches or response reaches. Transport reaches are delineated where the channel boundary is mixed bedrock and alluvium and/or the valley is confined and gradient controlled by bedrock (Figure 5). Transport reaches occur along the mainstem between USGS River Mile (RM) 104.4 and 91.3 (Doty and Leudinghaus Reaches) and between RM 89 and 87 (Lower Valley Reach). Surficial bed material in the Doty Reach is dominated by cobble and gravel bars with substantial areas of bedrock and boulder exposure, the Leudinghaus Reach is gravel dominated with approximately 30% cobble sized material and local bedrock exposures, and the Lower Valley Reach is gravel dominated with approximately 12 % cobble sized material.

Response reaches are defined where the channel boundary is primarily alluvium and channels free to migrate laterally across the valley bottom, typically forming a meandering planform (Figure 5). Two distinct response reaches were studied downstream of the mountain front on the mainstem Chehalis. The Ceres Hill Reach is positioned upstream of the confluence with the S. Fork between RM 91.3 and 87.7, and the Adna reach is located at the head of a continuous alluvial valley that extends downstream out of the study area to the vicinity of Centralia, where a bedrock knickpoint reduces the upstream gradient and prohibits downstream passage of gravel (Figure 1). Surficial bed material in the Ceres Hill Reach at present consists of ~95% gravel with significant overlying sand sheets, and in the Adna Reach consists of approximately 5% cobble material and 70-95% gravel, with the remainder sand. In addition, one response reach (Curtis) was studied on the South Fork Chehalis River downstream of the

confluence with Stillman Creek; the bed material in this reach is dominated by gravel with approximately 20% cobble sized material.

Results

Landslide Volume and Texture

The average slide depth of the 24 features measured was 1.8 m for debris slides and 2.0 m for debris torrents. The average amount of material from each slide that was estimated to be delivered to a stream was 57 percent for debris slides and 90 percent for debris torrents. Grain size samples of the landslide material indicate that 42% of the slide weight consisted of fines (sand and smaller), 46% consisted of gravel, and 12% consisted of cobble-sized material.

Application of this grain size distribution and these depths and delivery ratios results in the total estimated sediment yield to the channel network shown in Table 2. Specific event yields in the study area range from a minimum of 2,600 t km^{-2} on the S. Fork Chehalis River just above the confluence with Stillman Creek to 22,000 t km^{-2} where the mainstem Chehalis debouches from the mountains at Pe Ell. These volumes are extremely high compared to typical specific sediment yields of 140 to 1,300 t km^{-2} yr^{-1} for the basin area determined from suspended sediment measurements over the period 1962-1965 (Glancy 1971) and a 38-year record of landslide activity (Weyerhaeuser 1994a, 1994b).

Geomorphic Change by Reach

The following sections trace the impact of the slug, from headwaters reaches immediately below landslides, across zones of gravel deposition at the mountain front, and into distal reaches affected by finer grainsize fractions. The focus of the discussion is on geomorphic change in sedimentation zones, both at the mountain front and further downstream, although changes in selected transport zones where repeat LiDAR data were available are also considered. Changes in individual reaches described below exist within an overall pattern, which is illustrated in Figure 6. This figure, which in many ways is the central exhibit of this paper, summarizes patterns of deposition and erosion and changes in bank erosion rate and channel width through time.

Headwaters Reaches Channel Response

The active channel width in the S.F. Chehalis Headwate*rs* Reach increased from approximately 15 m in 2006 (or less, as much of the channel margin is obscured by canopy cover) in the available orthophoto to nearly 60 m as the entire valley bottom was inundated with sediment from debris flows and large wood rafts from both debris flow and local sources. In most areas of the reach, the low-flow channel was confined to a single thread in 2009, but patterns in the bar surface indicate that, during high flows, the entire valley bottom would be part of a braided channel (Figure 7a). By 2011, the average active channel width had contracted to less than 30 m, and by 2013 the channel had begun to downcut through the 2007 deposit, organizing the valley bottom into a distinct channel and floodplain (Figure 7b), with the channel returning to a width similar to the 2006 channel (10-15 m).

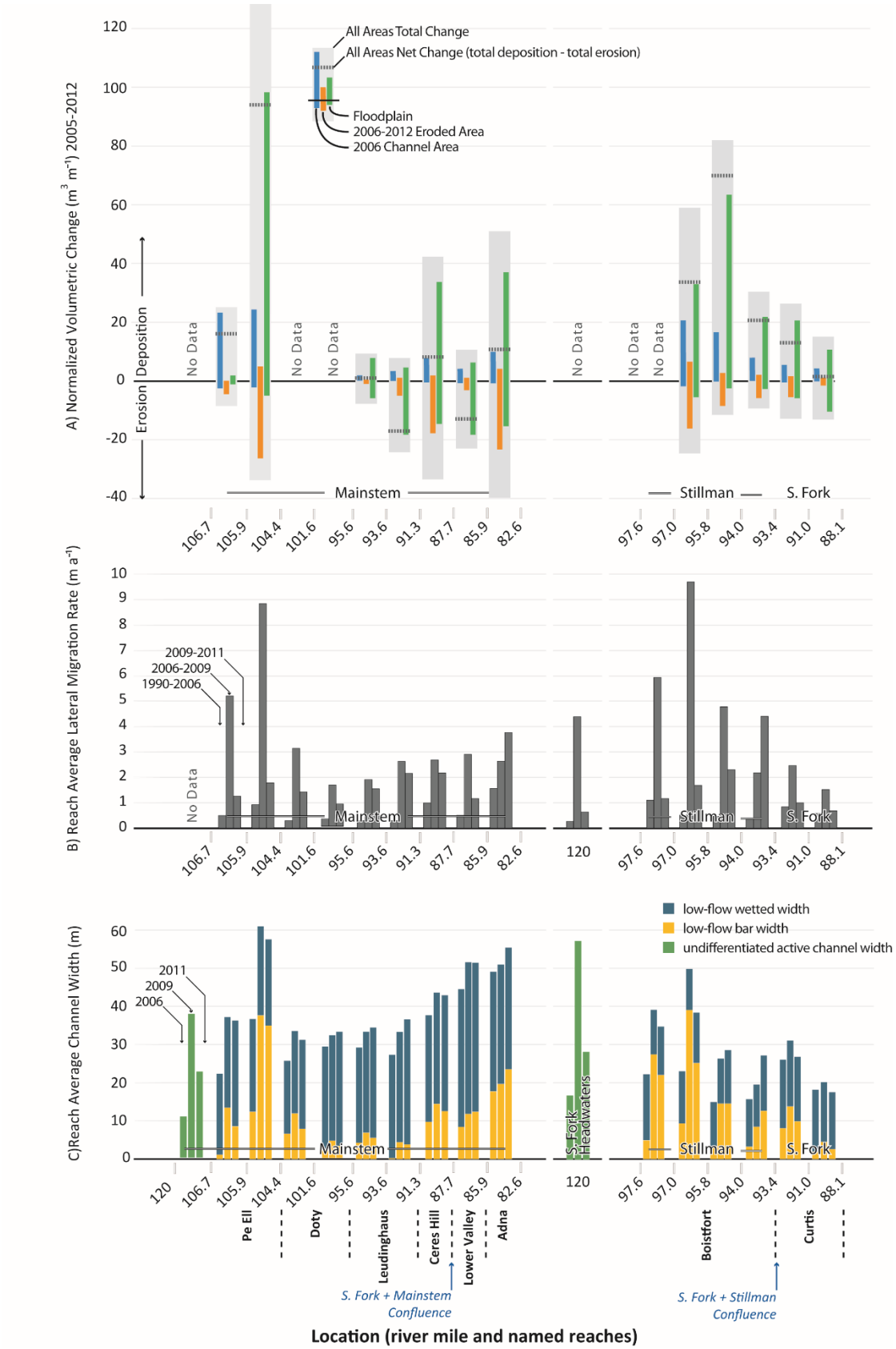

Figure 6: Summary of along-channel morphologic changes in the study area.

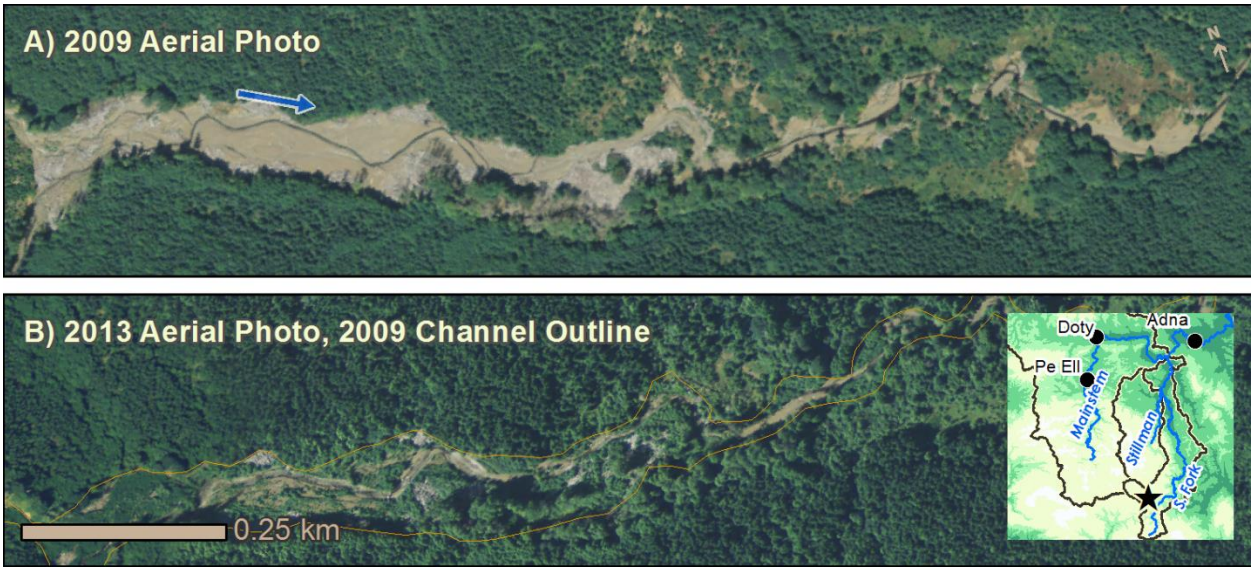

Figure 7: Aerial photos showing channel change in the S.F. Chehalis Headwaters Reach. Star on the inset location map shows the position of this reach in the basin.

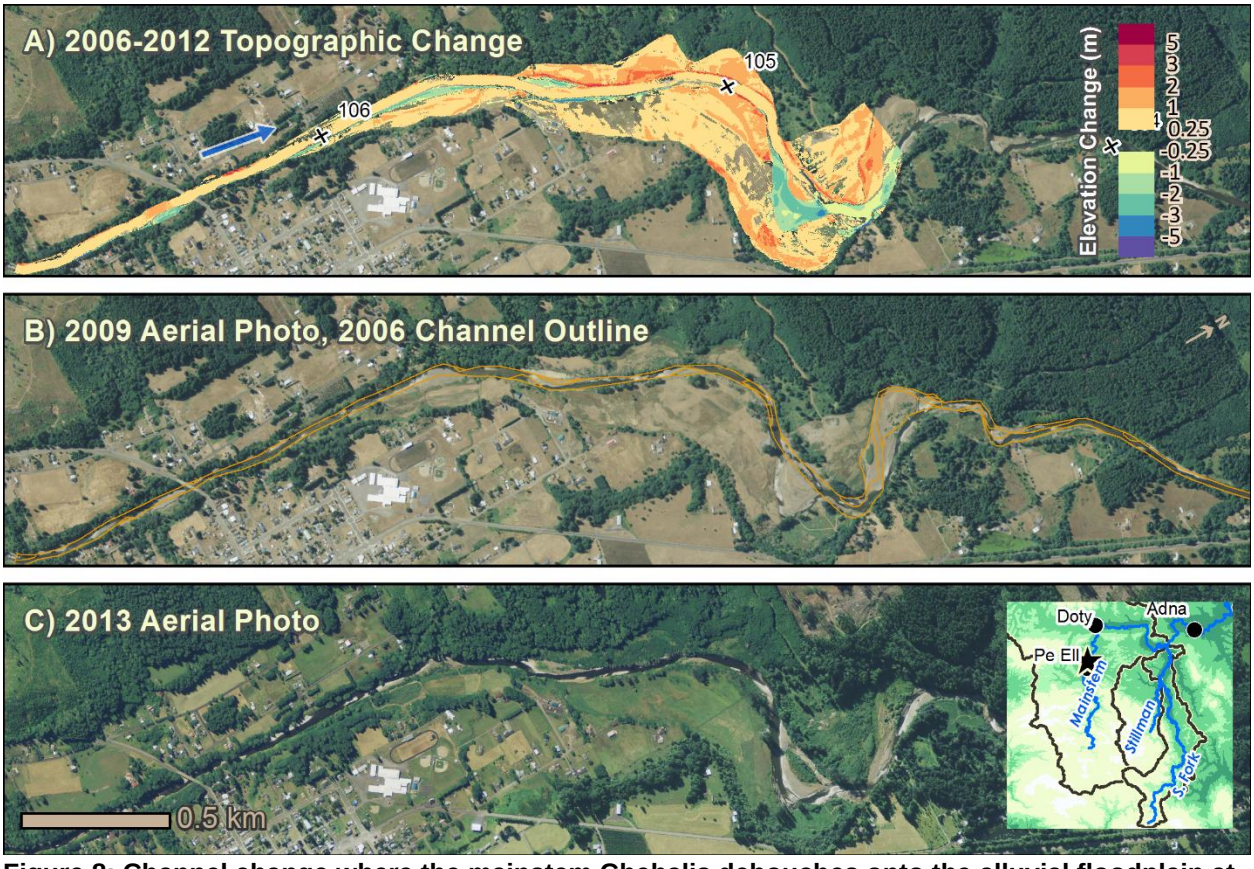

Figure 8: Channel change where the mainstem Chehalis debouches onto the alluvial floodplain at Pe Ell.

Mountain Front Channel Response

The most pronounced sedimentation of all reaches in the study area occurred on the mainstem Chehalis at Pe Ell (Figure 8). A total volume of 260,000 m^3 of material accumulated in this area, with a length-normalized net volumetric change of nearly 100 m^3 m^{-1} in the reach between RM 106 and 107 (Figure 6a). Gravel was deposited in the channel, leading to bar formation and (inferred) net bed aggradation, and 1-10 m per year reach-average lateral migration rates in the period 2006-2009 (Figure 6b) caused mostly by point-bar growth and reciprocal bank erosion but also some channel widening. Lateral migration rates decreased dramatically in the period from 2009-2011 following the pulse of sediment deposition. A large volume of sediment was deposited outside of the channel migration area and accumulated across the whole floodplain. The importance of bars in the morphologic structure of the river increased dramatically at Pe Ell; bar growth accounted for nearly all of 50-60% increases in channel width (Figure 6c).

In contrast to the mainstem Chehalis at Pe Ell, changes in slope and confinement are gradual along the Boistfort Reach of Stillman Creek. Additionally, there is no major valley constriction limiting the downstream extent of the sedimentation zone. These factors have resulted in less acute sediment accumulation over a much larger area along Stillman Creek (Figure 9). Length-normalized net volumetric change along Stillman Creek ranged from 20 to 65 m^3 m^{-1}, with peak deposition occurring 3-6 km

downstream of the alluvial fan head, and a downstream-skewed gamma-type distribution (Figure 6a). From the location of peak deposition downstream, the volume of sediment deposited on the floodplain dwarfed the volume of sediment deposited in the area where the channel migrated, while upstream lateral migration was more pronounced (6-10 m a^{-1} as opposed to 1.5-5 m a^{-1} downstream) and the volume of sediment deposited on point bars is comparable with the volume of sediment deposited on the floodplain. As with mountain front reaches at Pe Ell on the mainstem Chehalis, the influence of bars and active channel width both increased dramatically along Stillman Creek (Figure 6c). The wetted width at low flow decreased slightly. In areas upstream of the peak of sediment deposition, the width of the active channel began to contract in the period from 2009 to 2011, while downstream of the peak active channel width continued to increase (Figure 6c) and local erosion rates accelerated (Figure 6b).

Contraction of channel width and reduction of migration rates between 2009 and 2011 on the mountain-proximal reaches of both the mainstem Chehalis and Stillman Creek was accompanied by establishment of vegetation, stabilizing a very large proportion of the slug's total sediment volume in the floodplain.

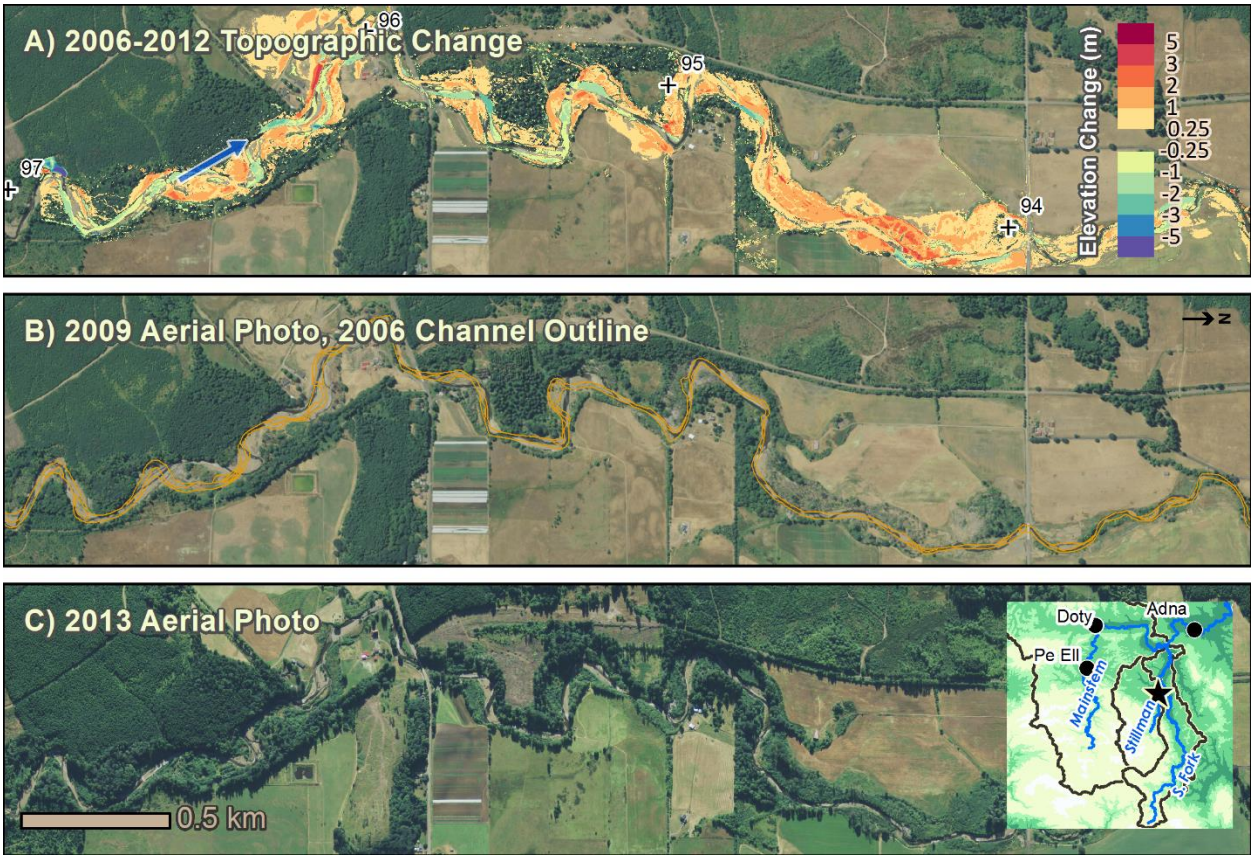

Figure 9: Channel change along the Stillman Creek alluvial fan.

Downstream Mainstem Reaches Channel Response

Important channel changes have also occurred downstream of the areas of maximum gravel and cobble deposition that are described above. In these areas, mechanisms forcing geomorphic change have included recent high water discharge, finer components of the landslide sediment (which may have been flushed rapidly through upstream reaches as suspended load), and locally derived sediment from bank erosion (which includes both gravel and fines). There is a distinct difference in the channel change in transport and response reaches. Channel alignment in transport reaches has been stable with net erosion caused by channel widening, while response reaches have

migrated laterally, eroding floodplain and/or terrace surfaces depositing material in growing point bars.

Transport Reaches

Downstream transport reaches all show very similar morphodynamic changes (Figure 10). Both reaches with repeat LiDAR coverage experienced net erosion caused by channel widening and slight erosion from floodplain surfaces (Figure 6). Notably, much of the erosion along these reaches occurred on the inside of bends. This is interpreted to indicate that the erosion was a regime adjustment to high flood discharges concentrated on areas where the channel margin was most erodible.

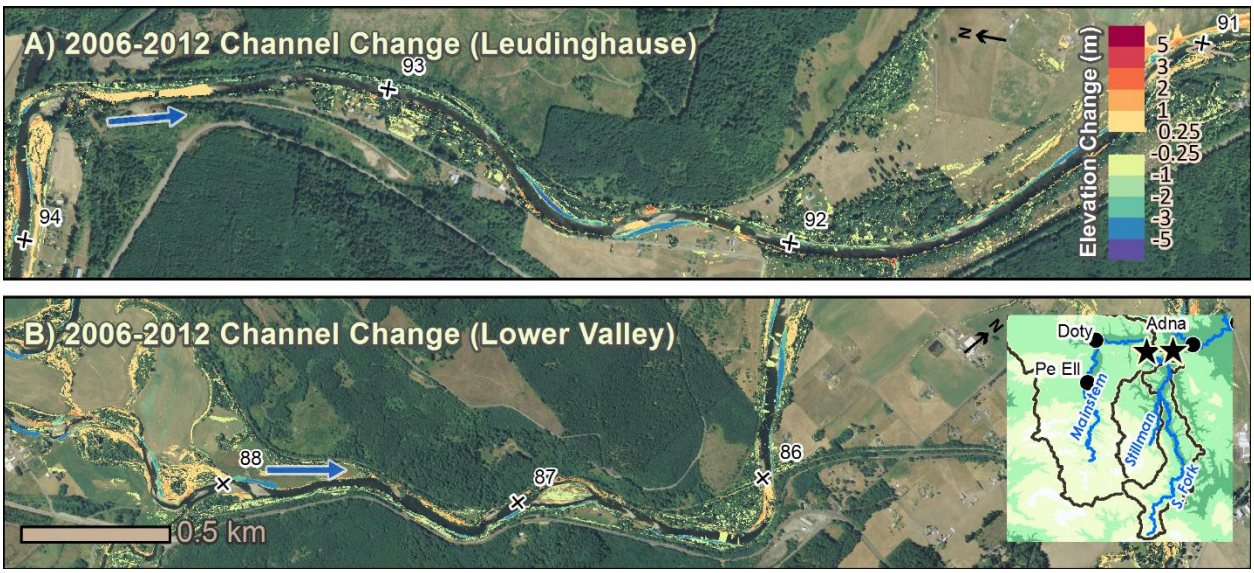

Figure 10: Geomorphic change along downstream transport reaches.

In the Doty Reach repeat LiDAR coverage is not available. Planimetric channel changes, however, are very similar to those in the Leudinghaus Reach just downstream (Figure 6b and 6c). The USGS gauge at Doty shows modest change accompanying the 2007 flood event, with specific gauge analysis indicating approximately 0.2 m of aggradation (Figure 11). In the Leudinghaus Reach, repeat LiDAR coverage shows very little growth of channel bars and floodplain erosion (in volumetric terms), relatively low bank erosion rates, and a slight (17%) increase in channel width, which was caused largely through erosion of the floodplain at the inside of point bars (Figure 10a) . The influence of bars in the reach grew substantially (from 15% to 20% of the active channel area).

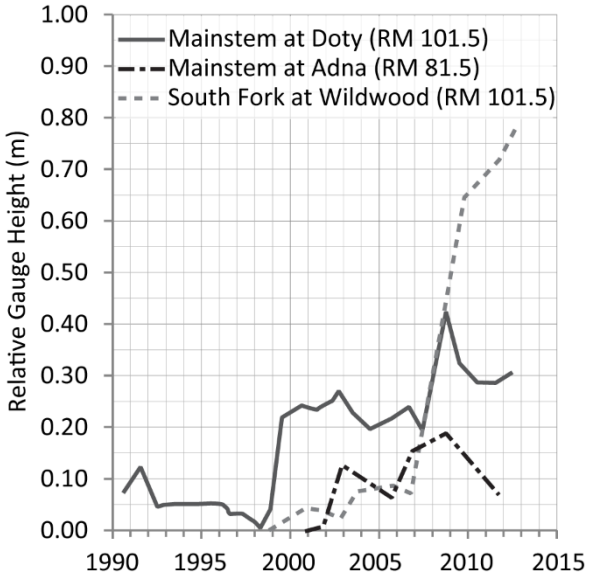

Figure 11: Specific gauge analysis for low flow conditions at gauges in the Upper Chehalis Basin ($1.7 < Q_w < 2.0$ m^3 s^{-1} at Doty for mainstem gauges and $0.4 < Q_w < 0.5$ m^3 s^{-1}at Wildwood gauge).

Response Reaches

Downstream response reaches on the mainstem Chehalis (Ceres Hill and Adna) saw net length normalized aggradation on the order of 10 m^3 m^{-1}. In these reaches erosion was concentrated at the outside of meander bends and in the floodplain along the edges of terraces. Deposition was concentrated on point bars reciprocal to bank erosion sites and also occurred in broad swaths across low-lying portions of the floodplain that had been inundated by flood waters (Figure 12 and Figure 13).\

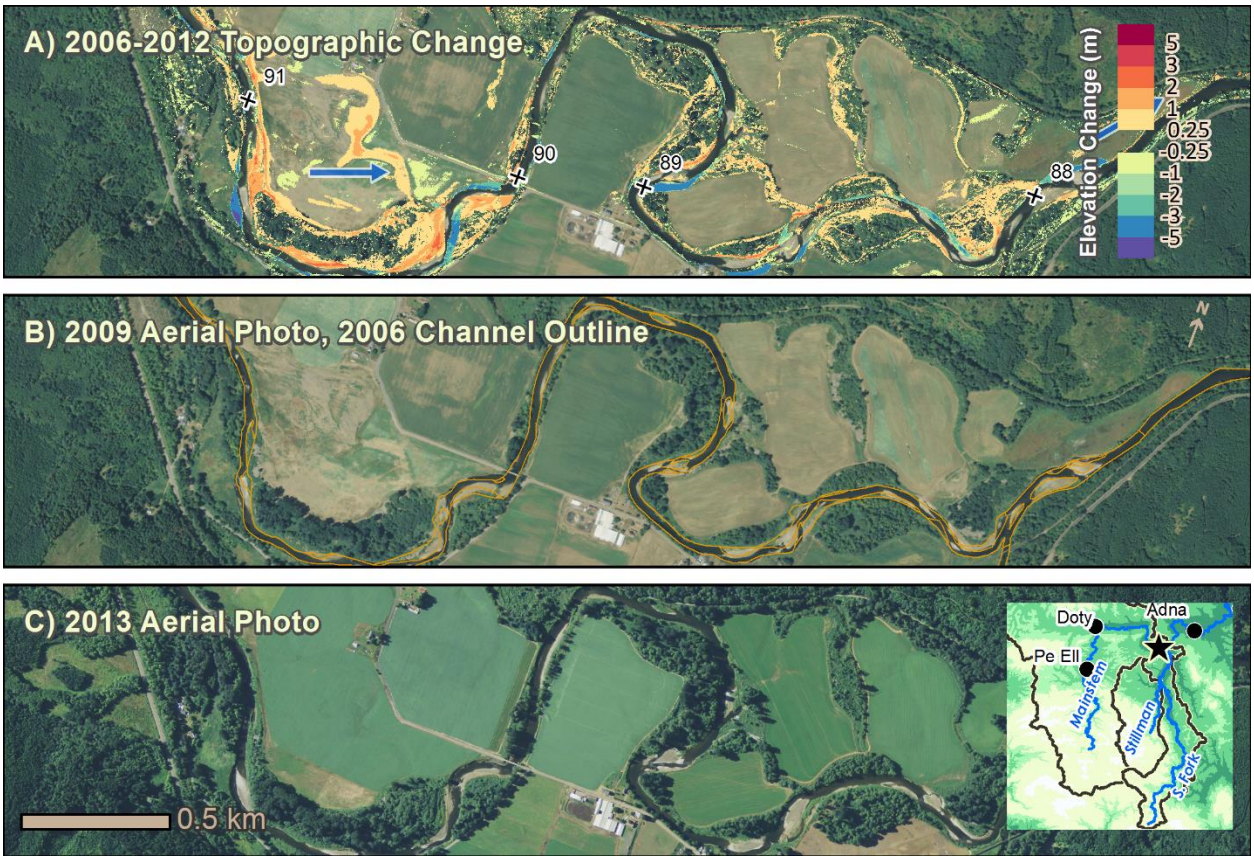

Figure 12: Geomorphic change along Ceres Hill response reach.

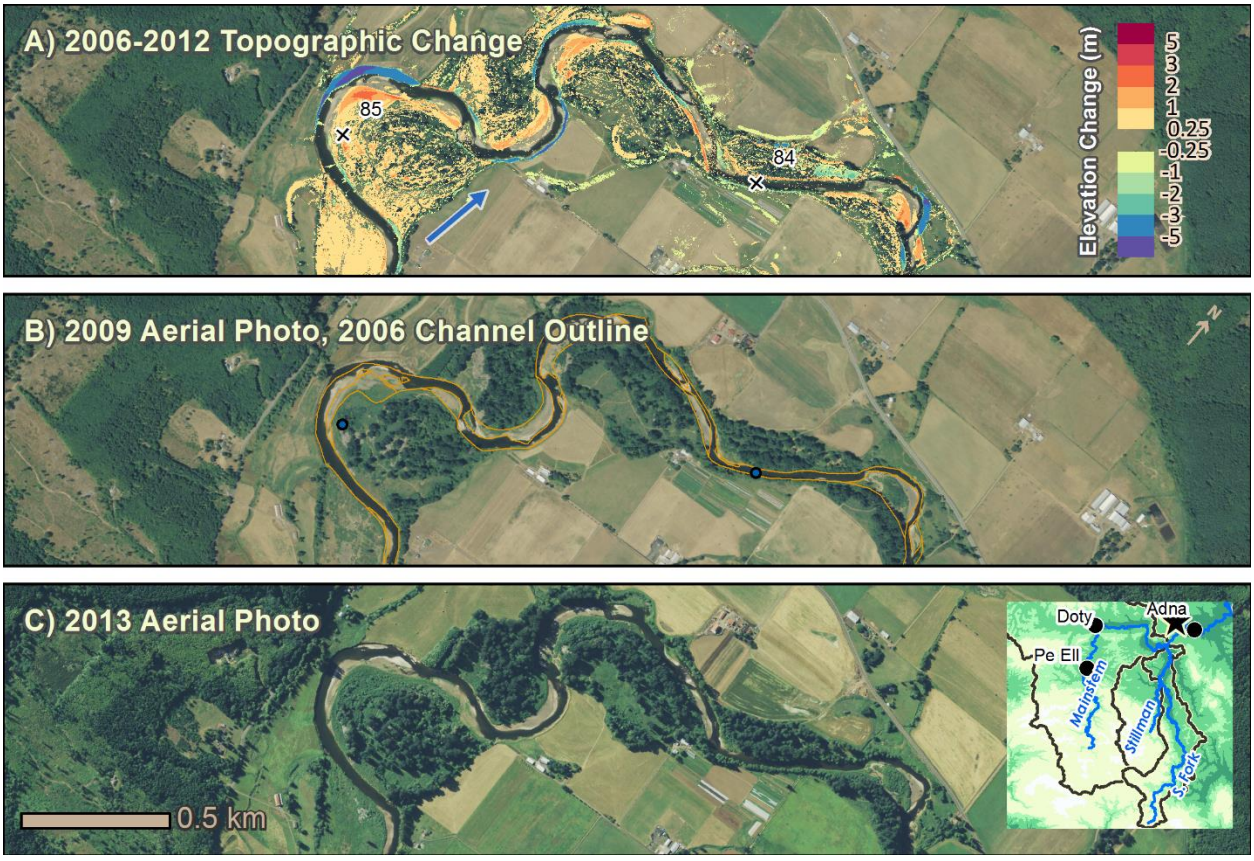

Figure 13: Geomorphic change along a portion of the Adana response reach.

Though bars in these reaches currently have a substantial fraction of surface sand (~5-10%) and are dominated by gravel, qualitative observations (Patricia Olsen, personal communication 2013) indicate that the texture of bars in these reaches changed from cobble- and gravel-dominated prior to the 2007 event to sand- and gravel after the event.

The average erosion rate in the Adna Reach increased from a baseline of 1.5 m a^{-1} (1990-2006) to 3 m a^{-1} over the period 2006-2009. In contrast to most other reaches in the study area, the erosion rate was faster between 2009 and 2011 (to 4 m a^{-1}) then it has been between 2006 and 2009. The width of the active channel and dominance of bars both increased (Figure 7c).

Eroding banks in downstream sedimentation reaches are typically on the order of 3 m higher than point bars growing across the river (Figure 5), and so even without channel widening, lateral migration erodes more volume of material from the floodplain than it deposits in bars within the active channel (Figure 6a), and net mobilization of sediment from the floodplain occurred due to channel migration. This imbalance was, however, more than compensated by accumulation fine sediment in low-lying floodplain areas, where up to 1.2 m of sediment was deposited, so that the overall change in storage in these reaches was positive.

Sediment Slug Dynamics

By integrating direct observations of morphologic change at the reach scale, and observing along-channel patterns of morphologic change (Figure 6), it becomes possible to make inferences about the large-scale dynamics of sediment slug behavior associated with the 2007 event.

Along Stillman Creek (and the S. Fork downstream of the confluence with Stillman), which flows in a gently concave channel crossing an alluvial fan with little non-alluvial constraint, the disturbance pattern is coherent: deposition volume, bank erosion rates, and changes in active channel width all resemble downstream-skewed gamma distributions. Peak planimetric disturbance measured by three metrics —reach average erosion rate (10 m a^{-1}), change in active width (91% increase), and proportion of the channel occupied by bars (38% increase) — occurred between RM 96 and 98 in the period 2006 to 2009. In these areas between 2009 and 2011, vegetation establishment on bars outpaced erosion of new floodplain, leading to a reduction in channel width and proportion of the channel occupied by bars. The peak rate of erosion between RM 93.4

and 94 occurred between 2009 and 2011; this is interpreted to indicate advancement of the leading wave of the gravel portion of the slug. If that interpretation is correct, than the virtual velocity of gravel composing the wave front was approximately 1.4 km a^{-1}.

Maximum aggradation along Stillman Creek between 2006 and 2012 occurred between RM 94 and 95.8, downstream of the maximum planmetric instability (RM 95.8-97), indicating a virtual velocity for the peak of the sediment wave of approximately 1.0 km a^{-1}. In the region of maximum aggradation, the lateral position of the active channel has remained relatively stable, but the channel has aggraded 0.6-1 m and 1.5-3 m thick sheets of gravel have been discharged onto the floodplain.

In contrast, the pattern of disturbance is relatively disordered along the mainstem Chehalis, where the long profile and valley width are influenced by bedrock. Transport reaches, where the channel is confined, were stable or showed net erosion due to channel widening. Sedimentation reaches, with broad alluvial floodplains, all showed substantial aggradation.

Observations of the bed material in the channel and channel's morphodynamic response allow inference of the current (as of 2013 aerial photo) position of the sediment slug in the system. The leading front of the gravel portion of the sediment slug has progressed approximately 25 km from the mountain front in the mainstem Chehalis River and 10 km from the mountain front in Stillman Creek; while the peak of disturbance has moved 8 km through the Chehalis River downstream of the mountain front and 3 km down Stillman Creek. The influence of sand mobilized by the landslides has reached much further downstream, with the leading edge of disturbance moving out of the study area (>50 km from the mountain front) and the peak of disturbance

occurring ~30-40 km from the mountain front along the mainstem Chehalis River. On Stillman Creek, the sand component of the wave has progressed into the S. Fork Chehalis River approximately 15 km from the mountain front and the peak of disturbance is approximately 10 km from the mountain front. Comparison of these slug propagation rates for the mainstem Chehalis River and Stillman Creek with theoretical predictions confirms the important control channel scale exerts over sediment slug propagation rate. Beechie (2001) suggests that sediment waves in gravel bed rivers should move at approximately a rate of 20 times the bankfull width of the channel annually, which on the mainstem Chehalis would translate to a rate of approximately 0.75 km a^{-1} and on Stillman Creek would translate to a rate of 0.45 km a^{-1}. The observed rates of the peak of the slug's disturbance are roughly similar to these theoretical predictions (20 to 75% higher) while the leading edge of the slug has propagated much further downstream.

It is possible to construct rough sediment budgets considering the total estimated landslide volume, connectivity between landslides and the channel network, grainsize distribution of the source sediment, and volume of aggradation downstream of the mountain front, as outlined in Table 3. Most of the sediment moved by landslides in the Stillman Creek basin was remobilized and moved to the mountain front (75%), while a relatively small component of the material in the mainstem Chehalis River basin was transported downstream to the mountain front (19%). If it is assumed that the fraction of connected landslide volume moved to the mountain front on Stillman Creek provides a minimum estimate of the fraction of connected landslide volume initially entrained by streams in the mainstem Chehalis basin, then it is possible to estimate that at least 30%

of the connected landslide volume is coarse material that remains in storage along the mainstem Chehalis above Pe Ell.

Discussion

Sediment Slug Evolution

The introduction of a bed material sediment slug coupled with highly energetic flood flows drove major geomorphic change in the upper Chehalis basin during and after the December 2007 storm. Here we have focused on quantifying the geomorphic response of channel units impacted by the flood and sediment slug, using coupled aerial photo-based channel mapping and multitemporal LiDAR data bracketing the event. While most case histories of comparable events have focused on reconstruction from landscape and archival evidence, here remote sensing data are available showing the evolution and impact of a large sediment slug in fine detail. The subsequent discussion is structured following the evolution of the slug as it moves down valley and interacts with peculiarities of the channel network and considering impacts in various affected environments.

First we consider the importance of medium to long term storage of the slug's sediment in headwaters reaches, as illustrated by channel dynamics in the S.F. Headwaters Reach and sediment budget. Valley-inundation promoted valley wide aggradation, and the channel subsequently incised through this deposit, returning toward pre-disturbance channel dimensions and presumably grade. In areas of relatively wide valley bottoms (Such as the S.F. Headwaters Reach) this resulted in storage of large volumes of sediment while in canyons and confined valleys only channel grade adjustments

occurred. Much previous work has shown that sediment yield after landscape-scale disturbances typically decays exponentially over a period of decades to centuries, with half-lives for the remaining volume of material initially disturbed ranging from approximately 5 to 50 years in established examples (Adams, 1980; Pearce and Watson, 1986; Major et al., 2000; Dadson et al., 2004; Koi et al., 2008; Hovius et al., 2011; Huang and Montgomery, 2012), where half-life ($t_{1/2}$) is computed as:

$$t_{1/2} = \frac{t \log 2}{\log\left[\frac{V_i}{V_f}\right]}. \quad (2)$$

The variable *t* represents the elapsed time of observation and V_i and V_f represent the initial landslide volume and landslide volume remaining in the upstream basin at the time of observation, respectively.

The pattern of exponential decay occurs because material mobilized by the disturbance becomes progressively more difficult for alluvial streams to reach as the most accessible deposits are carried away and as all deposits become stabilized through the formation of lag-armour deposits and establishment of vegetation. The sediment budgets constructed here allow calculation of the volume of sediment remaining in headwaters reaches of both Stillman Creek and the mainstem Chehalis, and therefore, the half-lives for alluvial export of landslide sediment from the headwaters. In the smaller and steeper Stillman Creek basin, where there is very little area like that illustrated by the S.F. Headwaters Reach, the half-life for storage of connected landslide sediment in the headwaters is extremely short —calculated as to be 2.4 years using the values of connected landslide volume and remaining storage in Table 3. In the large

mainstem Chehalis basin, where the channel gradient is lower and the valley bottom has substantially more area for alluviation, the half-life is longer (17 yrs), but still relatively short compared to the examples cited above. The comparatively high rate of sediment export and short half-lives observed in the present study are likely results of the extremely high flow that accompanied initial sediment production.

Next consider the system downslope at the mountain front reaches. The contrasting response of the Boistfort Reach on Stillman Creek and Pe Ell Reach on the mainstem Chehalis illustrate Hooke's (2003) framework for understanding coarse sediment connectivity. At the several-year timescale of this study, connectivity of the coarse (cobble-gravel) component of landslide material has been governed by both the virtual velocity of the sediment slug, and the movement of a large fraction of the total slug material into long-term storage in channel floodplains in mountain front sedimentation zone reaches. The material has been moved into storage by several factors. Channel aggradation occurred due to overwhelming sediment supply and a pattern of downstream-reduction in sediment transport capacity. This, in turn, caused a large volume of bed material to spill into overbank areas. On Stillman Creek this pattern was dominated by gradual downstream reduction in sediment transport capacity, while along the mainstem Chehalis, local constrictions (including bedrock, temporary large wood jams (Entrix, 2009), and bridges) resulted in both more pronounced local aggradation and strong patterning of transport- and response-reaches.

Both mountain front reaches show that even in the midst of slug passage, the volume of sediment aggraded in the channel is dwarfed by the volume of overbank storage (Figure 6a). Such overbank storage is a key mechanism in James' (2006, 2010) Gilbert Wave

model. This storage will regulate the long-term supply of sediment from the slug to downstream reaches. Gradual reworking of sediment stored in the floodplain will occur as the channels migrate, and will mete out sediment from the 2007 slug for a long period (decades to centuries) into the future during individual high flow events.

On the mainstem Chehalis, some volume of smaller grainsize fractions moved through the Pe Ell Reach at the mountain front and were flushed rapidly through transport reaches great distances downstream. This highly mobile material (some fraction potentially moving as washload through upstream reaches) passed to downstream sedimentation zone reaches where it settled to the bed and caused major change in channel form and migration rate. Thus, this case study highlights the importance of considering the potential for sorting mechanisms and grainsize specific transport pathways for the understanding of sediment wave evolution, in particular sediment waves may influence multiple zones along a river profile concentrated in regions where transport mechanisms change.

It may be particularly instructive to contrast the pattern of storage in the study area with that occurring after the historic dam removals on the Elwha River. Both slugs abruptly introduced on the order of 10 times the typical volume of alluvial sediment. The slug in the Elwha system evolved as a typical dispersive sediment wave (e.g. Lisle et al., 2001), with a limited volume of storage occurring only within the channel (East et al., 2014; Warrick et al., 2015), while in the present case a large fraction of the total slug volume moved into long-term storage on the floodplains. Peak flows on the Elwha during the study period reported by East et al. (2014) and Warrick et al. (2015) were approximately half of a two-year recurrence interval flood, and so the river was not

hydraulically connected to the floodplain to facilitate lateral sediment movement. In the present case, the combined effects of a high-magnitude flood, in-channel aggradation, and large wood jams created strong channel-floodplain connectivity and resulted in Gilbert Wave-like sediment slug evolution.

Channel Response to Elevated Bed Material Transport and High-Magnitude Flood

Finally, it is possible to consider what lessons may be learned from this case study considering the linkage between sediment and water supply and channel form and morphodynamics. Generally for sand and gravel-bedded rivers, increased sediment supply increases channel width and dominance of alluvial bars, often resulting in formation of braided planform (Church, 2006). Further, while it has generally been accepted that increased sediment supply results in decreased channel stability, recent research has shown quantitatively that lateral channel mobility (that is, the rate of lateral channel migration causing reworking of the floodplain surface, including erosion and formation of islands and floodplain areas) is positively correlated with increasing bedload flux over a broad range of channel forms (Wickert et al., 2013; Constantine et al., 2014).

High-magnitude floods alone, however, can trigger substantial geomorphic change (Schumm and Lichty, 1965; Everitt, 1968; e.g. Burkham, 1972; Costa, 1974; Gupta and Fox, 1974; Stevens et al., 1975; Wolman and Gerson, 1978; Osterkamp and Costa, 1987; Pizzuto, 1994; Costa and O'Connor, 1995; Hooke, 1996; Lane and Richards, 1997; Friedman and Lee, 2002). But in the present case, increased sediment supply

and the occurrence of an extreme flow must have acted together to trigger the observed responses. The extreme flow provided the energy needed to effectively move and redistribute sediment, probably increasing the quantity of sediment mobilized into the main branches from low-order tributaries, the quantity of sediment conveyed downstream, and rate at which the slug advanced downstream above that which could have occurred given only typical flood flows. Conversely, elevated sediment supply probably somewhat altered the impact of the extreme flood, especially in areas close to the mountain front. Debris delivered from upstream choked the channel during floods, and increased flow depths outside the channel to the point that these flows were competent to emplace a large volume of the bedload mixture on floodplain surfaces.

Observations of channel changes in the project area are consistent with the existing theoretical framework. Channel migration rates increased by a factor of 10 in the mountain front gravel sedimentation zones, and by a factor of 1-5 in downstream areas, including both sedimentation and transport reaches (Figure 14 A). Notably, although absolute rates were relatively modest, erosion rates in transport reaches increased proportionally more than in sedimentation zones. At the peak of slug impact, the active channel widened by 50 to >100% in mountain front reaches and by 10 to 20% in downstream sedimentation reaches (Figure 14 B). Nearly all of this widening was manifested as an increase in the dominance of active bars; in sedimentation zones, bars typically grew into the wetted channel and caused reciprocal bank erosion, while in transport reaches the floodplain along the inside of point bars eroded, allowing channel widening without shifting the thalweg. On average across all studied reaches, bar dominance increased from approximately 20% to 40% of the active channel, with the

greatest increase (from 5 and 20 % to 30 and 50%, respectively) in reaches closest to the mountain front, through which the greatest amount of bed material was conveyed (Figure 14 C).

By calculating the volume of downstream deposition, it is possible to estimate the minimum bed material flux into and through a particular reach in the study area. By doing this, the geographic patterns observable in Figure 14 can be generalized. Figure 15 shows correlations between bed material transport into a reach (normalized to basin area) and change in three dependent geomorphic parameters: bank erosion rate, active channel width, and proportion of the active channel occupied by bars. All three dependent parameters show a strong correlation to the bed material flux through the reach. The relation between erosion rate and bed material flux confirms the result of Wickert et al. (2013) in a field environment very different then that considered by Constantine et al. (2014) and further strengthens the case that bed material sediment flux is one of the fundamental driving forces behind channel migration. The relationships between change in active channel width and proportion of the active channel occupied by bars also correlate tightly to bed material flux through the reach, providing additional empirical support for the notion that increased non-cohesive sediment supply will increase channel width and the dominance of alluvial bars (e.g. Church, 2006).

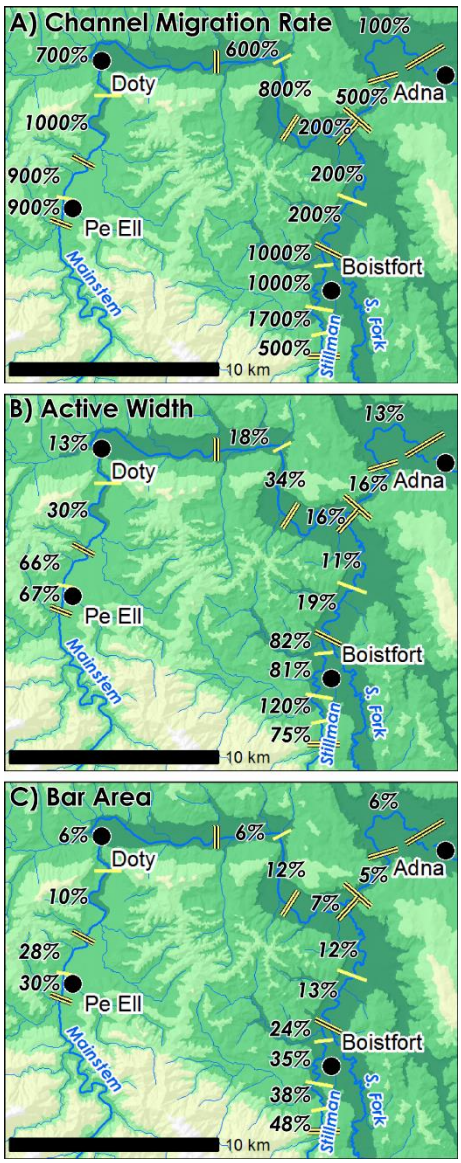

Figure 14: A) percent increase in erosion rate during slug passage over 1990-2006 baseline, B) percent increase in active channel width during slug passage compared to 2006 condition, C) change in percent of active channel occupied by bars during slug passage compared to 2006 condition.

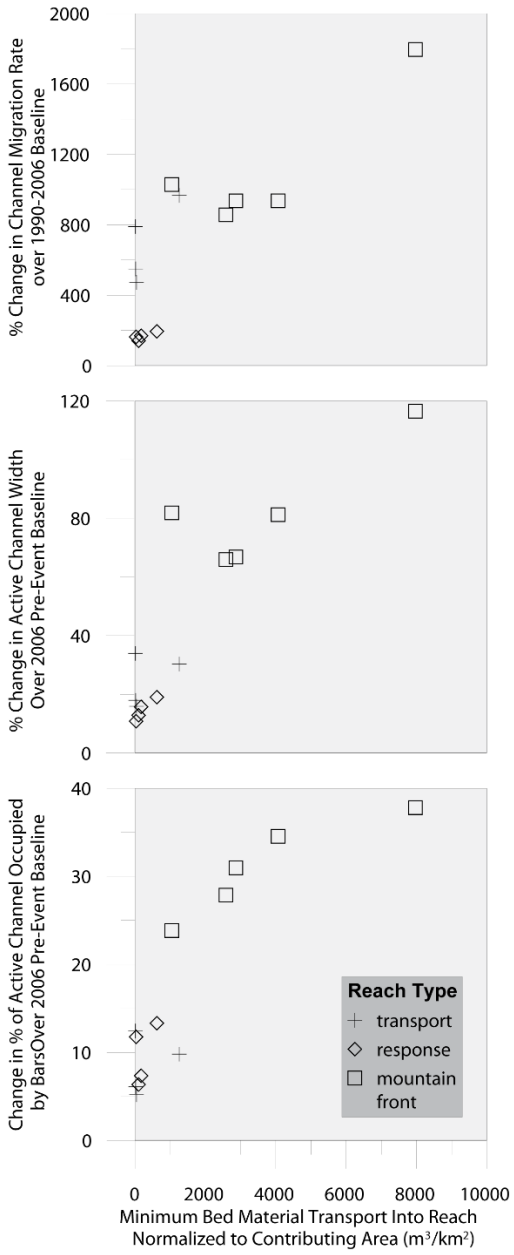

Figure 15: Correlations between bed material transport into a reach and change in bank erosion rate, active channel width, and proportion of the active channel occupied by bars. The normalization of bed material transport volume by contributing area facilitates comparison to the dependent variables, which are all measures of change relative to a baseline condition: by normalizing to basin area, the independent variable becomes a measure of change from typical bed material transport rates assuming a baseline relation of bed material transport rate and basin area.

Conclusion

Two broad themes have been considered in this paper: the dynamic evolution of sediment slugs acting as Gilbert Waves moving through one relatively simple (Stillman Creek) and one complex (mainstem Chehalis) channel network and the impact of that elevated bed material transport on channel form and lateral mobility. Downstream attenuation in the wave volumes occurred because large volumes of material were exported from the channel to the valley bottom, providing stores of material that may be reworked for decades or centuries to come. The particular patterns of this slug emplacement responded to the peculiarities of the flood hydrology and channel and valley form; a coherent pattern of disturbance is evident along Stillman Creek, while the mainstem Chehalis is divided into highly responsive sedimentation zones and transport reaches that appear to have rapidly flushed the slug sediment downstream. Dramatic increases in channel lateral mobility, active channel width, and the relative dominance of alluvial bars all occurred in response to the event. Though high flows were likely important in providing the competence to move large volumes of sediment, close correlations between bed material sediment flux through reaches and their geomorphic response highlight the important role bed material flux plays governing channel form and driving rates and patterns of morphodynamic processes.

Acknowledgements

This paper reports work completed in part with funding and support from the Washington State Legislature through the Chehalis River Basin Flood Authority, and

Northwest Hydraulic Consultants. The authors gratefully acknowledge helpful comments that improved the manuscript provided by Michael Church and Joanna Curran.

References

Adams J. 1980. Contemporary uplift and erosion of the Southern Alps, New Zealand. Geological Society of America Bulletin **91** : 1–114.

Beechie TJ. 2001. Empirical predictors of annual bed load travel distance, and implications for salmonid habitat restoration and protection. Earth Surface Processes and Landforms **26** : 1025–1034. DOI: 10.1002/esp.251

Benda L, Dunne T. 1997. Stochastic forcing of sediment routing and storage in channel networks. Water Resources Research **33** : 2865–2880. DOI: 10.1029/97WR02387

Burkham DE. 1972. Channel changes of the Gila river in Safford valley, Arizona, 1846-1970

Church M. 2006. Bed Material Transport and the Morphology of Alluvial River Channels. Annual Review of Earth and Planetary Sciences **34** : 325–354. DOI: 10.1146/annurev.earth.33.092203.122721

Constantine JA, Dunne T, Ahmed J, Legleiter C, Lazarus ED. 2014. Sediment supply as a driver of river meandering and floodplain evolution in the Amazon Basin. Nature Geoscience **7** : 899–903. DOI: 10.1038/ngeo2282

Costa JE. 1974. Response and recovery of a Piedmont watershed from tropical storm Agnes, June 1972. Water Resources Research **10** : 106–112.

Costa JE, O'Connor JE. 1995. Geomorphically effective floods. Natural and anthropogenic influences in fluvial geomorphology : 45–56.

Croke J, Fryirs K, Thompson C. 2013. Channel-floodplain connectivity during an extreme flood event: implications for sediment erosion, deposition, and delivery: CHANNEL-FLOODPLAIN CONNECTIVITY. Earth Surface Processes and Landforms : n/a–n/a. DOI: 10.1002/esp.3430

Cui Y, Parker G, Lisle TE, Gott J, Hansler-Ball ME, Pizzuto JE, Allmendinger NE, Reed JM. 2003. Sediment pulses in mountain rivers: 1. Experiments. Water Resources Research **39** : n/a–n/a. DOI: 10.1029/2002WR001803

Dadson SJ et al. 2004. Earthquake-triggered increase in sediment delivery from an active mountain belt. Geology **32** : 733–736.

DNR. 2008. Resource Arial Photography Lewis County 2008 [online] Available from: http://www.dnr.wa.gov/BusinessPermits/Topics/Maps/Pages/resource_aerial_photography.aspx

DNR. 2010. Landslides [online] Available from: http://www.dnr.wa.gov/ResearchScience/Topics/GeosciencesData/Pages/gis_data.aspx (Accessed 1 April 2013)

East AE et al. 2014. Large-scale dam removal on the Elwha River, Washington, USA: River channel and floodplain geomorphic change. Geomorphology DOI: 10.1016/j.geomorph.2014.08.028 [online] Available from: http://linkinghub.elsevier.com/retrieve/pii/S0169555X14004553 (Accessed 26 September 2014)

Entrix. 2009. Assessement of the December 2007 Flood Event in the Upper Chehalis Basin . Washington Forest Law Center [online] Available from: http://umcatel.weyerhaeuser.com/NewSustainability/pdfs/Entrix%20report.pdf (Accessed 21 January 2014)

Everitt BL. 1968. Use of the cottonwood in an investigation of the recent history of a flood plain. American Journal of Science **266** : 417–439.

Friedman JM, Lee VJ. 2002. Extreme floods, channel change, and riparian forests along ephemeral streams. Ecological Monographs **72** : 409–425.

Gesch D, Evans G, Mauck J, Hutchinson J, Carswell Jr WJ. 2009. The national map: Elevation. US geological survey fact sheet **3053** [online] Available from: http://pubs.usgs.gov/fs/2009/3053/ (Accessed 31 March 2015)

Gran KB, Montgomery DR. 2005. Spatial and temporal patterns in fluvial recovery following volcanic eruptions: Channel response to basin-wide sediment loading at Mount Pinatubo, Philippines. Geological Society of America Bulletin **117** : 195–211.

Gupta A, Fox H. 1974. Effects of high-magnitude floods on channel form: A case study in Maryland Piedmont. Water Resources Research **10** : 499–509.

Hoffman DF, Gabet EJ. 2007. Effects of sediment pulses on channel morphology in a gravel-bed river. Geological Society of America Bulletin **119** : 116–125. DOI: 10.1130/B25982.1

Hooke J. 2003. Coarse sediment connectivity in river channel systems: a conceptual framework and methodology. Geomorphology **56** : 79–94. DOI: 10.1016/S0169-555X(03)00047-3

Hooke JM. 1996. River responses to decadal-scale changes in discharge regime: the Gila River, SE Arizona. Geological Society, London, Special Publications **115** : 191–204. DOI: 10.1144/GSL.SP.1996.115.01.15

Hovius N, Meunier P, Lin C-W, Chen H, Chen Y-G, Dadson S, Horng M-J, Lines M. 2011. Prolonged seismically induced erosion and the mass balance of a large earthquake. Earth and Planetary Science Letters **304** : 347–355.

Huang MY-F, Montgomery DR. 2012. Fluvial response to rapid episodic erosion by earthquake and typhoons, Tachia River, central Taiwan. Geomorphology **175-176** : 126–138. DOI: 10.1016/j.geomorph.2012.07.004

James A. 2010. Secular Sediment Waves, Channel Bed Waves, and Legacy Sediment: Secular sediment waves and legacy sediment. Geography Compass **4** : 576–598. DOI: 10.1111/j.1749-8198.2010.00324.x

James LA. 1989. Sustained storage and transport of hydraulic gold mining sediment in the Bear River, California. Annals of the Association of American Geographers **79** : 570–592.

James LA. 1991. Incision and morphologic evolution of an alluvial channel recovering from hydraulic mining sediment. Geological Society of America Bulletin **103** : 723–736.

James LA. 1993. Sustained reworking of hydraulic mining sediment in California: GK Gilbert's sediment wave model reconsidered. Zeitschr. Geomorphol. Suppl **88** : 49–66.

James LA. 2006. Bed waves at the basin scale: implications for river management and restoration. Earth Surface Processes and Landforms **31** : 1692–1706. DOI: 10.1002/esp.1432

Jones JL. 2006. Side channel mapping and fish habitat suitability analysis using lidar topography and orthophotography. Photogrammetric Engineering and Remote Sensing **72** : 1202.

Klingeman PC, Emmett WW. 1982. Gravel bedload transport processes. Gravel-Bed Rivers: Fluvial Processes, Engineering and Management, RD Hey, JC Bathurst, and CR Thornes (Editors). John Wiley, New York, New York : 141–169.

Koi T, Hotta N, Ishigaki I, Matuzaki N, Uchiyama Y, Suzuki M. 2008. Prolonged impact of earthquake-induced landslides on sediment yield in a mountain watershed: The Tanzawa region, Japan. Geomorphology **101** : 692–702. DOI: 10.1016/j.geomorph.2008.03.007

Kuo C-W, Brierley G. 2014. The influence of landscape connectivity and landslide dynamics upon channel adjustments and sediment flux in the Liwu Basin, Taiwan: LANDSCAPE CONNECTIVITY AND CHANNEL ADJUSTMENTS IN THE LIWU BASIN. Earth Surface Processes and Landforms **39** : 2038–2055. DOI: 10.1002/esp.3598

Lane SN, Richards KS. 1997. Linking river channel form and process: time, space and causality revisited. Earth Surface Processes and Landforms **22** : 249–260.

152 Lingley L, Slaughter S, Sarikhan I, Norman D. 2013. Comparison of slope instability
153 screening tools following a large storm event and application to forest management and
154 policy (Discussion of). Geomorphology **184** : 151–153. DOI:
155 10.1016/j.geomorph.2012.01.001

156 Lisle TE, Cui Y, Parker G, Pizzuto JE, Dodd AM. 2001. The dominance of dispersion in
157 the evolution of bed material waves in gravel-bed rivers. Earth Surface Processes and
158 Landforms **26** : 1409–1420. DOI: 10.1002/esp.300

159 Logan R. 1987. Geologic map of the Chehalis River and Westport Quadrangles,
160 Washington [online] Available from: http://www.dnr.wa.gov/Publications/ger_ofr87-
161 8_geol_map_chehalisriver_westport_100k.zip

162 Major JJ. 2004. Posteruption suspended sediment transport at Mount St. Helens:
163 Decadal-scale relationships with landscape adjustments and river discharges. Journal
164 of Geophysical Research: Earth Surface (2003–2012) **109** [online] Available from:
165 http://onlinelibrary.wiley.com/doi/10.1029/2002JF000010/full (Accessed 12 February
166 2014)

167 Major JJ, Janda RJ, Daag AS. 1996. Watershed disturbance and lahars on the east
168 side of Mount Pinatubo during the mid-June 1991 eruptions. Fire and mud: Eruptions
169 and lahars of Mount Pinatubo, Philippines : 895–919.

170 Major JJ, Pierson TC, Dinehart RL, Costa JE. 2000. Sediment yield following severe
171 volcanic disturbance—a two-decade perspective from Mount St. Helens. Geology **28** :
172 819–822.

173 Marron DC. 1992. Floodplain storage of mine tailings in the belle fourche river system:
174 A sediment budget approach. Earth Surface Processes and Landforms **17** : 675–685.
175 DOI: 10.1002/esp.3290170704

176 Meade RH. 1982. Sources, Sinks, and Storage of River Sediment in the Atlantic
177 Drainage of the United States. The Journal of Geology **90** : 235–252.

178 Mote P, Mault J, Duliere V. 2008. The Chehalis River flood of December 3-4, 2007 .
179 Office of Washington State Climatologist: University of Washington [online] Available
180 from:
181 http://www.climate.washington.edu/events/dec2007floods/OWSC_Chehalis_Dec08_Flo
182 od_Report.pdf

183 Nelson AD, Church M. 2012. Placer mining along the Fraser River, British Columbia:
184 The geomorphic impact. Geological Society of America Bulletin **124** : 1212–1228.

185 Nicholas AP, Ashworth PJ, Kirkby MJ, Macklin MG, Murray T. 1995. Sediment slugs:
186 large-scale fluctuations in fluvial sediment transport rates and storage volumes.
187 Progress in Physical Geography **19** : 500–519. DOI: 10.1177/030913339501900404

188 Osterkamp WR, Costa JE. 1987. Changes accompanying an extraordinary flood on a
189 sand-bed stream. Catastrophic flooding **18** : 201–224.

190 Parker G, Klingeman PC, McLean DG. 1982. Bedload and size distribution in paved
191 gravel-bed streams. Journal of the Hydraulics Division **108** : 544–571.

192 Pearce AJ, Watson AJ. 1986. Effects of earthquake-induced landslides on sediment
193 budget and transport over a 50-yr period. Geology **14** : 52–55.

194 Pizzuto JE. 1994. Channel adjustments to changing discharges, Powder River,
195 Montana. Geological Society of America Bulletin **106** : 1494–1501.

196 PSLC. 2005. Lewis County Project, Bare Earth DEM

197 PSLC. 2012. Chehalis River Watershed Project

198 Sarikhan I, Stanton K, Contreras T, Polenz M, Powell J, Walsh T, Logan R. 2008.
199 Landslide Reconnaissance Following the Storm Event of December 1-3, 2007, in
200 Western Washington . Washington State Department of Natural Resources

201 Schumm SA, Lichty RW. 1965. Time, space, and causality in geomorphology. American
202 Journal of Science **263** : 110–119.

203 Stevens MA, Richardson EV, Simons DB. 1975. Nonequilibriun River Form. Journal of
204 the Hydraulics Division **101** : 557–566.

205 Sutherland DG, Ball MH, Hilton SJ, Lisle TE. 2002. Evolution of a landslide-induced
206 sediment wave in the Navarro River, California. Geological Society of America Bulletin
207 **114** : 1036–1048. DOI: 10.1130/0016-7606(2002)114<1036:EOALIS>2.0.CO;2

208 Turner TR, Duke SD, Fransen BR, Reiter ML, Kroll AJ, Ward JW, Bach JL, Justice TE,
209 Bilby RE. 2010. Landslide densities associated with rainfall, stand age, and topography
210 on forested landscapes, southwestern Washington, USA. Forest Ecology and
211 Management **259** : 2233–2247. DOI: 10.1016/j.foreco.2010.01.051

212 USDA NRCS. 2013. Soild Data Mart [online] Available from:
213 http://soildatamart.nrcs.usda.gov/. (Accessed 26 March 2015)

214 USGS. 2008. New Peak Flow For Record Chehalis Flood. United States Geological
215 Survey News Release 5th February [online] Available from:
216 http://wa.water.usgs.gov/news/2008/news.chehalis.newpeak.htm (Accessed 23 March
217 2015)

218 Walsh TJ. 1987. Geologic Map of the Astoria and Ilwaco Quadrangles, Washington and
219 Oregon [online] Available from: http://www.dnr.wa.gov/Publications/ger_ofr87-
220 2_geol_map_astoria_ilwaco_100k.zip

221 Warrick JA, Bountry JA, East AE, Magirl CS, Randle TJ, Gelfenbaum G, Ritchie AC,
222 Pess GR, Leung V, Duda JJ. 2015. Large-scale dam removal on the Elwha River,
223 Washington, USA: Source-to-sink sediment budget and synthesis. Geomorphology DOI:
224 10.1016/j.geomorph.2015.01.010 [online] Available from:
225 http://linkinghub.elsevier.com/retrieve/pii/S0169555X15000227 (Accessed 31 March
226 2015)

227 Wheaton JM, Brasington J, Darby SE, Merz J, Pasternack GB, Sear D, Vericat D. 2010.
228 Linking geomorphic changes to salmonid habitat at a scale relevant to fish. River
229 Research and Applications **26** : 469–486. DOI: 10.1002/rra.1305

230 Whittaker KA, McShane D. 2012. Comparison of slope instability screening tools
231 following a large storm event and application to forest management and policy.
232 Geomorphology **145-146** : 115–122. DOI: 10.1016/j.geomorph.2012.01.001

233 Wickert AD, Martin JM, Tal M, Kim W, Sheets B, Paola C. 2013. River channel lateral
234 mobility: metrics, time scales, and controls: RIVER CHANNEL LATERAL MOBILITY.
235 Journal of Geophysical Research: Earth Surface **118** : 396–412. DOI:
236 10.1029/2012JF002386

237 Wolman GM, Gerson R. 1978. Relative scales of time and effectiveness of climate in
238 watershed geomorphology. Earth Surface Processes **3** : 189–208.

239 Wolman MG. 1954. A method of sampling coarse river-bed materials. Transactions of
240 the American Geophysical Union **35** : 951–956.

241

Tables

Table 1: Aerial photo acquisition dates and river discharge.

Photo Acquisition Date	Chehalis mainstem Discharge at Doty ($m^3 s^{-1}$)
10-15 Jul, 1990	2.2
21 Jul, 2006	0.9
1 Aug, 2009	1.3
20 Aug, 2011	1.0
14 Aug, 2013	1.8

Table 2: Landslide volumes and sediment yields for the 2007 event compared with typical basin sediment yield.

Basin	Total Slide Volume (m^3)	Total Slide Weight (t)*	Specific Event Yield (t km^{-2})	Typical Sediment Yield (t km^{-2} yr^{-1})
Mainstem Chehalis	3,300,000	3,500,000	6,400 at S.F. Confluence 22,000 at Pe Ell	140 (1962-65) 1,300 (1955-1993)
S. Fork Chehalis	370,000	390,000	2,600 at Stillman Confluence	--
Stillman Creek	1,100,000	1,200,000	10,000 at S.F. Confluence	200 (1955-1993)
Total	4,900,000	5,100,000	6,300	

*Using bulk density **of 1.04 t m^{-3}** based on Natural Resources Conservation Service soil data for the study area

(NRCS 2012)

Table 3: Sediment budget for mountain front reaches and upstream basins.

Basin	Total Connected Landslide Volume (m^3)[A]	Downstream Aggradation (m^3)	Estimated Washload (42%)[B]	Upstream Connected Storage Remaining (m^3)[C]
Mainstem Chehalis	2,000,000	260,000	110,000	1,630,000
Stillman Creek	690,000	370,000	150,000	170,000

Notes: A) Volumes presented here are less than those in Table 2 because these are reduced to show only the estimated volume connected to stream channels and available for fluvial transport. B) This represents the volume of sand and finer material that must have been eroded from landslides to mobilize the deposited volume of gravel. C) This represents a maximum estimate because the volume of gravel transported downstream away from the mountain front reaches is unknown (though presumed small).